

NASA TECHNICAL NOTE



NASA TN D-5562

C.1

NASA TN D-5562



LOAN COPY: RETURN TO  
AFWL (WLOL)  
KIRTLAND AFB, N MEX

# BLADE-ELEMENT PERFORMANCE OF A TANDEM-BLADED INDUCER TESTED IN WATER

*by Richard F. Soltis, Donald C. Urasek, and Max J. Miller*

*Lewis Research Center*

*Cleveland, Ohio*

NATIONAL AERONAUTICS AND SPACE ADMINISTRATION • WASHINGTON, D. C. • NOVEMBER 1969



0132370

1. Report No. NASA TN D-5562 _____	2. Government Accession No. _____	3. Recipient's Catalog No. _____	
4. Title and Subtitle BLADE-ELEMENT PERFORMANCE OF A TANDEM- BLADED INDUCER TESTED IN WATER		5. Report Date November 1969	6. Performing Organization Code _____
7. Author(s) Richard F. Soltis, Donald C. Urasek, and Max J. Miller		8. Performing Organization Report No. E-4949	
9. Performing Organization Name and Address Lewis Research Center National Aeronautics and Space Cleveland, Ohio 44135		10. Work Unit No. 128-31	11. Contract or Grant No. _____
12. Sponsoring Agency Name and Address National Aeronautics and Space Administration Washington, D.C. 20546		13. Type of Report and Period Covered Technical Note	
15. Supplementary Notes _____			
16. Abstract A tandem-bladed inducer was tested in water. The three-bladed inducer was 6.5 in. (16.5 cm) in diameter at the inlet, and the blade sections were formed by radial elements. The design values of flow coefficient and head-rise coefficient were 0.109 and 0.303, respectively. The radial distributions of performance and flow parameters across the tandem-blade elements are presented for a range of flow rates under both non-cavitating and cavitating conditions. At design flow, the design level of head-rise coefficient was attained in the blade tip region. Measurements indicated that blade-element efficiencies varied from approximately 97 percent at the hub to 75 percent at the tip.			
17. Key Words (Suggested by Author(s)) Tandem inducer Blade-element performance		18. Distribution Statement Unclassified - unlimited	
19. Security Classif. (of this report) Unclassified	20. Security Classif. (of this page) Unclassified	21. No. of Pages 36	22. Price* \$3.00

\*For sale by the Clearinghouse for Federal Scientific and Technical Information  
Springfield, Virginia 22151

# BLADE-ELEMENT PERFORMANCE OF A TANDEM-BLADED INDUCER TESTED IN WATER

by Richard F. Soltis, Donald C. Urasek,  
and Max J. Miller

Lewis Research Center

## SUMMARY

A tandem-bladed inducer was tested in water. The three-bladed inducer was 6.5 inches (16.5 cm) in diameter at the inlet, and the blade sections were formed by radial elements. The design values of flow coefficient and head-rise coefficient were 0.109 and 0.303, respectively. In this report, the radial distributions of performance and flow parameters across tandem-blade elements are presented for a range of flow rates under both noncavitating and cavitating conditions.

At design flow, the inducer produced design head rise in the blade tip region. However, it produced a slightly lower head rise across the remaining portion of the blade span.

Near design operating conditions, the head rise of the tandem inducer, when compared with the head rise obtained with a typical flat-plate helical inducer, was found to be nearly twice the level attained with the flat plate inducer. The efficiency of the tandem inducer also remained higher across most of the blade passage.

Radial distributions of loss coefficient were apparently influenced by secondary flow effects. The loss coefficient increased significantly with radius at most flow rates. Blade-element efficiencies were inversely related to radius and varied from approximately 97 percent near the hub to 75 percent near the tip.

At flow coefficients less than 0.09, an eddy was detected in the tip region at the inducer inlet. The radial extent of the eddy increased as flow was reduced. One result of the eddy formation was a redistribution of flow that prevented excessive incidence angles from occurring in the lower portions of the blade span over the flow range studied.

Midspan noncavitating data were taken with the rear blade moved slightly to three different locations with respect to the front blade. As the overlap of the front and rear blades was increased, the measured losses decreased over the flow range studied.

# INTRODUCTION

The level of blade loading that can be applied efficiently to a given blade row depends primarily on the success in preventing the blade surface boundary layers from separating. One approach to exercising some control of blade surface boundary layer on highly loaded blade rows is to use tandem blades. In a tandem configuration, the high overall blade loading is apportioned to two or more close-coupled blade sections so that blade surface boundary layer separation is forestalled on any of the individual blades. The slot geometry formed by the two blades may be designed to direct some high-momentum fluid over the suction surface of the downstream blade to further aid in delaying boundary layer separation on this surface.

In many applications, the inducer of a pump is relatively lightly loaded to provide sufficient head rise to avoid cavitation in subsequent pumping stages. The tandem-blade concept suggests combining a lightly loaded upstream blade section for high suction performances with a highly loaded downstream blade section for high head rise. This approach has been applied to an inducer rotor designed for NASA under contract. A description of the inducer, its overall performance when operated in water, and visual observations with cavitating and noncavitating flow are presented in reference 1.

Herein, the radial variations of flow and performance parameters measured across tandem-blade elements at selected radial locations are presented for a range of operating conditions covering both noncavitating and cavitating flow. This type of data is useful in the analysis of the performance of the present design and in the design of similar tandem-blade sections. The data also indicate the radial distributions of flow conditions that a downstream stator blade row would have to accept over the operating range. The effects of small changes in slot geometry on the performance parameters for the midspan blade elements are also shown.

## APPARATUS AND PROCEDURE

### Test Pump

The following inducer design specifications were dictated by the existing test facility:

Inlet tip diameter, $d_t$ , in. (cm) . . . . .	6.5 (16.5)
Inlet hub-tip radius ratio, $r_h/r_t$ . . . . .	0.4
Ratio of inducer outlet area to inlet area, $A_2/A_1$ . . . . .	0.5
Maximum axial depth, in. (cm) . . . . .	4.5 (11.4)

(Symbols are defined in appendix A.) The outer casing at the test section incorporated a linear taper from a diameter of 6.5 inches (16.5 cm) near the inducer inlet to a diameter of 6.175 inches (15.7 cm) near the outlet. The inducer tip diameter was matched to this taper.

The following hydrodynamic design values were supplied by the designer:

Ideal inlet flow coefficient $\phi_{id}$ . . . . .	0.109
Head-rise coefficient $\psi$ . . . . .	0.303

As discussed in reference 2, the inlet flow coefficient, when combined with an  $r_h/r_t$  of 0.4 and an inlet flow angle  $\beta_1$  of  $0^\circ$ , is the optimum value for a suction specific speed of approximately 30 000.

The inducer had three tandem blades (see fig. 1). Each tandem blade was composed of a relatively long-chord front blade (7.74 in. or 19.66 cm at tip) and a short-chord

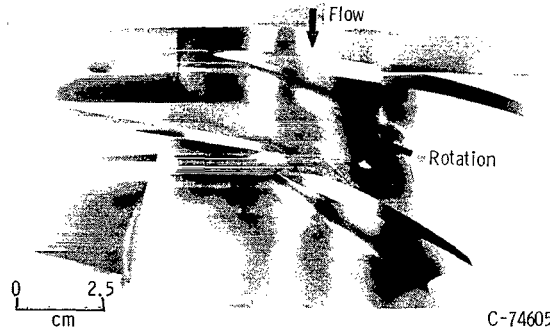


Figure 1. - Tandem-bladed inducer.

rear blade (2.75 in. or 6.98 cm at tip). The front and rear blades were fabricated individually from separate material blanks. This permitted some freedom to vary the relative circumferential position of the trailing and leading edges of the two blades during testing. The hub radius increased across the inducer as needed to meet the required area change and comply with the specified tip taper. A blade tip clearance of 0.015 inch (0.038 cm) was used.

In the blade design procedure, only the blade-section geometry for the element on the tip diameter cylindrical surface ( $d_c = 6.5$  in. or 16.5 cm) for both blades is specified. The remaining blade sections are defined by radial lines from this tip section. The geometry of the blade tip section for both front and rear blades is given in figure 2. The blade suction and pressure surfaces are helical surfaces with different leads that have curved surfaces in the inlet region as defined by given coordinate schedules. The two helical surfaces are separated by a specified thickness value. The fairing of the

Rear blade						Front blade					
Directional coordinate											
x		y		-y		x		y		-y	
in.	cm	in.	cm	in.	cm	in.	cm	in.	cm	in.	cm
0	0	0.042	0.107	0.042	0.107	0	0	0.039	0.099	0.039	0.099
.055	.140	.074	.188	.023	.058	.010	.025	.046	.117	.026	.066
.108	.274	.094	.239	.018	.046	.150	.381	.087	.221	.015	.038
.240	.610	.135	.343	.009	.023	.215	.546	.103	.262	.009	.023
.381	.968	.166	.422	.002	.005	.320	.813	.122	.310	.004	.010
.520	1.321	.183	.465	0	0	.500	1.270	.143	.363	0	0
.790	2.007	.204	.518			.950	2.413	.169	.429		
1.050	2.667	.203	.516			1.300	3.302	.180	.457		
1.431	3.635	.180	.457			2.030	5.156	.191	.485		
						2.790	7.087	.194	.493		
						3.550	9.017	.178	.452		
						7.640	19.406	.081	.206		

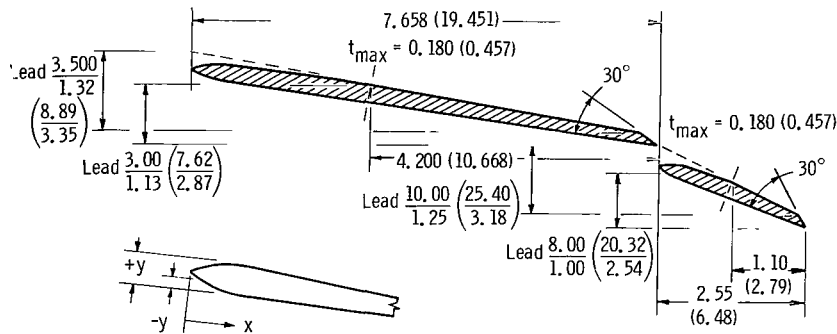


Figure 2. - Blade section (front and rear blades) at 6.5-inch (16.51-cm) tip diameter. Leading edge radius, 0.010 inch (0.025 cm). (All dimensions are in inches (cm).)

pressure surfaces of both front and rear blades is very small in the chordwise direction so that these surfaces remain essentially a flat plate. The fairing of the suction surface extends over approximately the forward half of the blade section. Thus, in this forward portion of the blade section, a locus of midpoints between pressure and suction surfaces would describe a line with some camber. The blade was fabricated with nearly a constant thickness from hub to tip.

### Test Facility

The tandem-bladed inducer was tested in the Lewis waterpump test facility. A sketch of this closed-loop test facility is shown in figure 3. Prior to testing, the water is circulated through the degasifying and filtering system. The gas content is reduced and maintained at less than 3 ppm by weight, and the filter is capable of removing particles over 5 micrometers. The test facility is discussed in more detail in reference 3.

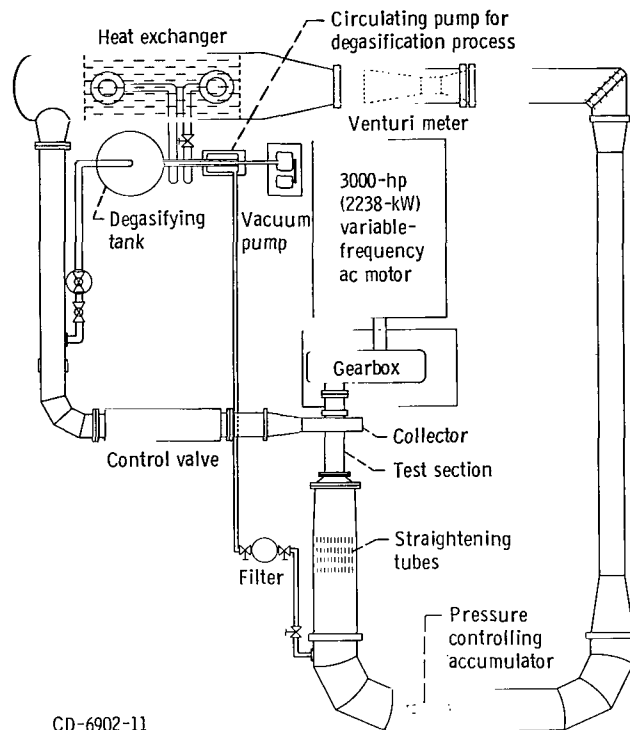


Figure 3. - Lewis water tunnel.

## Test Procedure and Instrumentation

Flow conditions were measured at the inducer inlet and outlet (approx 0.5 in. or 1.27 cm upstream and downstream of the blade leading and trailing edges, respectively). The inducer was operated (1) over a range of flow rates at constant values of rotative speed and net positive suction head  $H_{SV}$  and (2) over a range of net positive suction heads at constant values of rotative speed and flow. Design rotative speed was 5415 rpm. Survey probes measured total pressure, static pressure, and flow angle at radial positions located at 10, 30, 50, 70, and 90 percent of the annulus height from the outer wall. The equations used to calculate selected flow and performance parameters are presented in appendix B.

The survey probes are shown in figure 4. Total pressure and flow angle were measured with the cobra probe (fig. 4(a)) and static pressure with the wedge probe (fig. 4(b)). Each probe had associated null-balancing, stream-direction-sensitive equipment that automatically alined the probe to the direction of flow. Each wedge static probe was calibrated in a low-speed air tunnel. Flow rate was measured with a Venturi flowmeter, and rotor rotative speed was measured with a magnetic pickup coupled to an electronic speed counter.

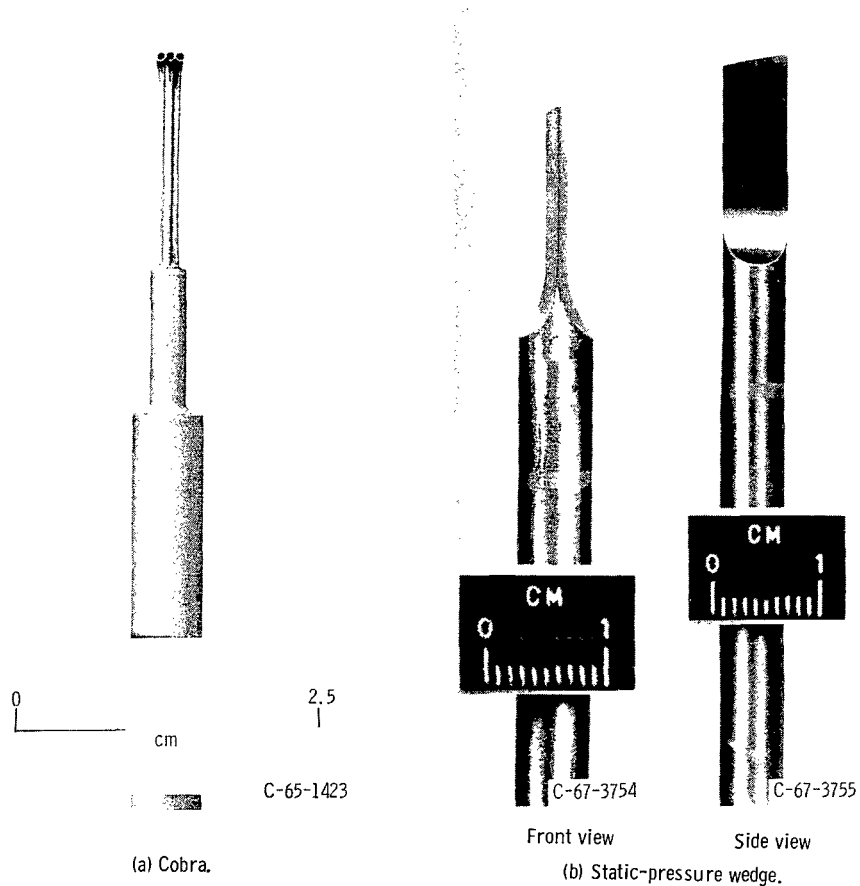


Figure 4. - Probes.

### Data Accuracy and Reliability

Errors in the data due to the inherent inaccuracies of the measurement and recording systems are estimated to be as follows:

Flow rate, $Q_v$ , percent of design flow . . . . .	$\pm 1.0$
Rotative speed, $N$ , percent . . . . .	$\pm 0.5$
Head rise, $\Delta H$ , percent at design flow . . . . .	$\pm 1.0$
Velocity head, $V^2/2g$ , percent at design flow . . . . .	$\pm 1.5$
Flow angle, $\beta_1$ , deg . . . . .	$\pm 1.0$
Net positive suction head, $H_{sv}$ , ft (m) . . . . .	$\pm 1.0 (\pm 0.31)$

The influence of unsteady flows, circumferential variations in flow, and other time or space gradients could not be evaluated. However, preliminary measurements indicated that the circumferential variations of flow conditions at the rotor outlet were small and that the flow could be considered axisymmetric (see ref. 1).

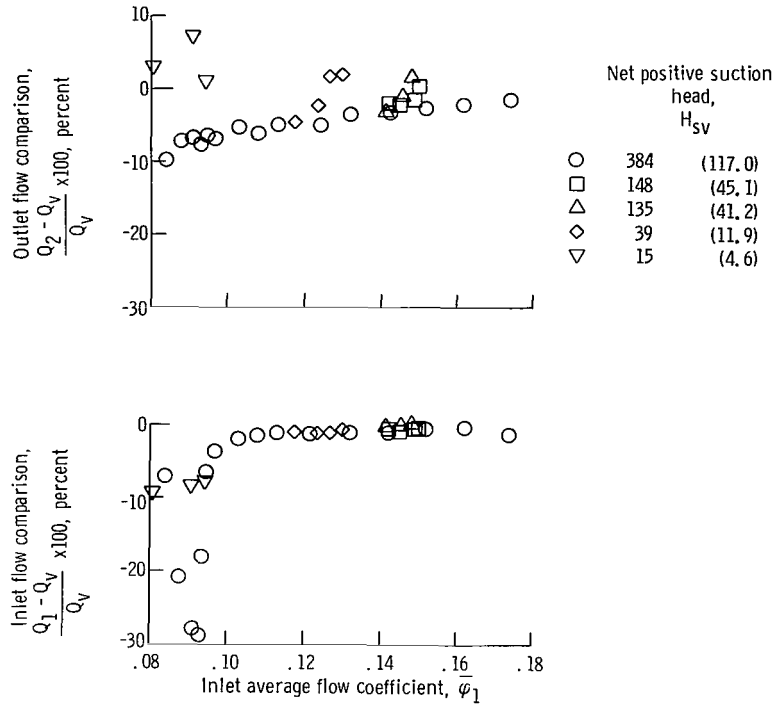


Figure 5. - Comparison of integrated flows at inducer inlet and outlet with those measured by Venturi meter.

A measure of the accuracy of the data is also provided by comparing the flow rates, as determined from the integrated survey measurements at the inlet and outlet of the inducer, to the flow rate measured with the Venturi meter. The flow comparisons are presented in figure 5 in the forms

$$\frac{Q_1 - Q_v}{Q_v} \times 100$$

and

$$\frac{Q_2 - Q_v}{Q_v} \times 100$$

and are plotted as a function of average inlet flow coefficient  $\bar{\varphi}_1$ . At flow coefficients greater than 0.10, the integrated flows at the inducer inlet are within 2 percent of the Venturi flows for all levels of  $H_{sv}$ . At flow coefficients less than 0.10, the integrated flows deviate significantly from the Venturi flows. This deviation is attributed to a re-

verse flow region that forms in the inlet tip region at  $\bar{\varphi} < 0.10$  and makes it difficult to obtain a meaningful integration of flow. Also, at the low inlet pressures, cavitation forms on the wedge static probe.

At the inducer outlet, the integrated flows compare with the Venturi flows within a few percent at the high flows. As the flow is reduced, the deviation of the two flow measurements increases consistently to values of approximately 7 percent. Some of this percentage increase between the two flow calculations is expected because of the combination of lower through-flow velocities and a measuring system with a fixed inherent accuracy. In general, the flow checks indicate a reasonable agreement of measured data.

## Blade-Element Parameters

The blade-element parameters selected to describe the flow conditions and performance across the individual blade elements include (1) inlet flow coefficient,  $\varphi_1$ , (2) incidence angle,  $i$ , (3) loss coefficient,  $\bar{\omega}$ , (4) diffusion factor,  $D$ , (5) outlet absolute flow angle,  $\beta_2$ , (6) turning angle,  $\Delta\beta'$ , (7) outlet flow coefficient,  $\varphi_2$ , (8) ideal head-rise coefficient,  $\psi_{id}$ , (9) actual head-rise coefficient,  $\psi$ , and (10) hydraulic efficiency,  $\eta$ . The definitions of the parameters are given in appendixes A and B. Velocity diagrams at the inlet and outlet may be computed, if desired, from flow coefficient, flow angle, and local blade speed.

Of primary interest are the head-rise coefficient  $\psi$  and the efficiency  $\eta$  of the flow process. The blade-element head rise is equal to the energy addition (indicated by the ideal head-rise coefficient  $\psi_{id}$ ) minus the flow losses (indicated by the loss coefficient  $\bar{\omega}$ ). Efficiency is the ratio of the head-rise coefficient to the ideal head-rise coefficient. The energy addition is affected by the blade speed  $U$ , the fluid turning angle  $\Delta\beta'$ , and the outlet axial velocity (indicated by flow coefficient  $\varphi_2$ ). The energy addition increases with an increase in blade speed, an increase in fluid turning angle, and a decrease in outlet flow coefficient. The flow losses across a blade element are assumed to be influenced primarily by (1) incidence angle of the entering flow, (2) blade loading level, and (3) secondary flows. The flow incidence angle is related to the magnitude of the rapid accelerations and decelerations of the flow around the leading edge region of the blade. These local flow decelerations have attendant diffusion losses together with losses due to possible local boundary layer separation and reattachment. The blade loading level gives a measure of the blade surface velocity gradients and the associated diffusion loss, friction loss, and possible losses due to boundary layer separation.

Herein, the diffusion factor  $D$  gives a measure of the blade loading. A development of this parameter is given in reference 4. Secondary flows are flows occurring in the low-momentum boundary layers (both on the blade surface and the casing walls) because of the pressure gradients imposed on them by the main flow through the blade passage. These secondary flows include a passage secondary flow, centrifuging of blade surface boundary layer, blade tip clearance flows, blade trailing vortices, and so forth. The energy associated with these secondary flows is not recoverable and thus becomes a loss. These relations briefly summarize the blade-element parameters. Flow conditions for all the blade elements are related by the need to satisfy the requirements of radial equilibrium and continuity.

The incidence angle  $i$  is defined as the difference between the flow direction and a tangent to the blade mean line at the blade leading edge, or  $i = \beta'_1 - \kappa_1$ . From the description of blade shape in the section Test Pump and the sketches in figure 2, it can be seen that a mean line direction in the blade leading edge region is not defined analytically. For the tip blade section (shown in fig. 2), a mean line direction  $\kappa_t$  at the leading edge was determined graphically. For all other elements, the blade camber angle at the leading edge was computed from

$$\kappa_n = \tan^{-1} \left[ \left( \frac{r_n}{r_t} \right) \tan \kappa_t \right]$$

The most easily defined surface of the blade section is the helix surface forming the blade pressure surface. Very little contouring of this profile is done in the leading edge region (see fig. 2). For this surface, the front blade inlet angle is

$$\kappa_n = \tan^{-1} \frac{2\pi r_n}{\text{lead}} = \tan^{-1} \frac{2\pi r_n}{3.0}$$

TABLE I. - BLADE INLET ANGLES

Span from hub, percent	Blade angle, $\kappa$ , deg	
	Mean camber line	Pressure surface
90	86.3	81.1
70	86.0	79.8
50	85.6	78.1
30	85.1	75.8
10	84.4	72.6

The blade inlet angles calculated by both of the foregoing methods are presented in table I for the five radial locations at which data were taken.

## RESULTS AND DISCUSSION

The performance of the inducer is presented first in terms of its noncavitating, or base, performance levels. Cavitating performance is presented and discussed in terms of the effects of cavitation on this base performance.

### Noncavitating Performance

Overall performance. - The noncavitating overall performance is presented in figure 6, where average values of head-rise coefficient  $\bar{\psi}$  and hydraulic efficiency  $\bar{\eta}$  are

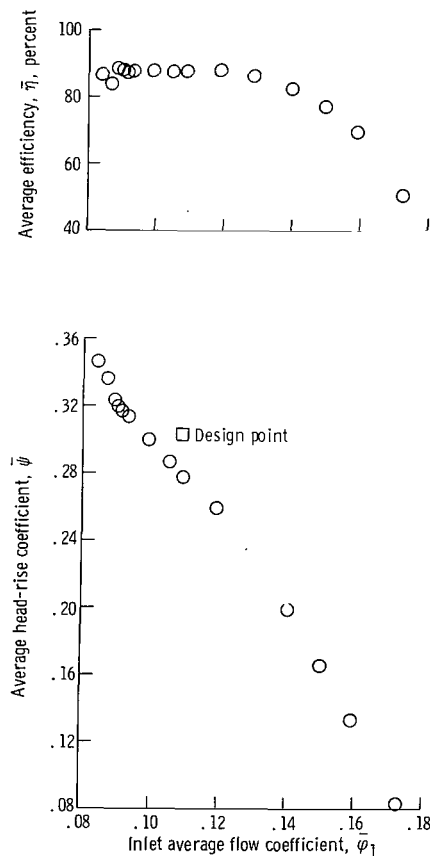


Figure 6. - Inducer overall performance at noncavitating conditions. Net positive suction head, 384 feet (117 m).

shown as functions of average inlet flow coefficient  $\bar{\varphi}_1$ . The head-rise coefficient and efficiency are mass-averaged values. The inlet flow coefficient is based on the measured flow and the inlet geometric area. The equations for computing these values are given in appendix B.

The overall performance is discussed in reference 1. It is included in this report to indicate the overall performance level that results from a summation of the performance of the individual blade elements and to indicate the relation of the operating point at which blade-element data are presented to the overall operating range covered.

An inlet flow blockage of 2.2 percent, due to hub and tip casing boundary layers, was computed near design flow (see ref. 1). Thus, the design inlet ideal flow coefficient of 0.109 will actually be achieved at an overall measured flow coefficient  $\bar{\varphi}_1$  of

$$\bar{\varphi} = 0.978 \bar{\varphi}_{id} = (0.978)(0.109) = 0.107$$

Comparisons of measured flow conditions with design are made at an overall inlet flow coefficient of 0.107. At a  $\bar{\varphi}$  of 0.107, the inducer achieved an overall head-rise coefficient of 0.282 (as compared with the design value of 0.303) and had an overall efficiency of 88 percent. The plots of figure 6 also show that a relatively high efficiency (>80 percent) was maintained over the greater portion of the flow range.

At a  $\bar{\varphi}$  of approximately 0.09, sharp increases in flow angle and total head were noted in the tip region (90 percent of passage height from the hub) at the inlet measuring station, as shown in figure 7. For further flow reductions, limit switches on the probe actuators prevented the probe from turning past an angle of about  $100^\circ$ . As flow was reduced from a flow coefficient of 0.09, similar increases in flow angle were noted at radial stations 70 and 50 percent of the passage height from the hub. These angle measurements observed at the three radial locations are interpreted as an indication of the formation and radial growth of a reverse flow, or eddy, in the blade tip region. As shown by the visualization techniques discussed in reference 1, tufts mounted on the outer casing indicated a flow directly into the inducer ( $\beta_1 = 0$ ) at high flows and a  $180^\circ$  change in direction of flow at  $\bar{\varphi}$  less than 0.09.

The increases in inlet total head indicate some energizing of the eddy flow. This could result from fluid entering the rotating passages, being energized, and flowing back out into the inlet, or it could result from the viscous action of the eddy flow to induce a tangential component to the inlet flow.

Blade-element performance. - Performance and flow parameters are computed for five blade elements. Herein a blade element, or flow streamline, is assumed to pass through radial locations the same percentage of passage height at the blade inlet and outlet measuring stations. Such an approach provides a reasonable approximation to actual

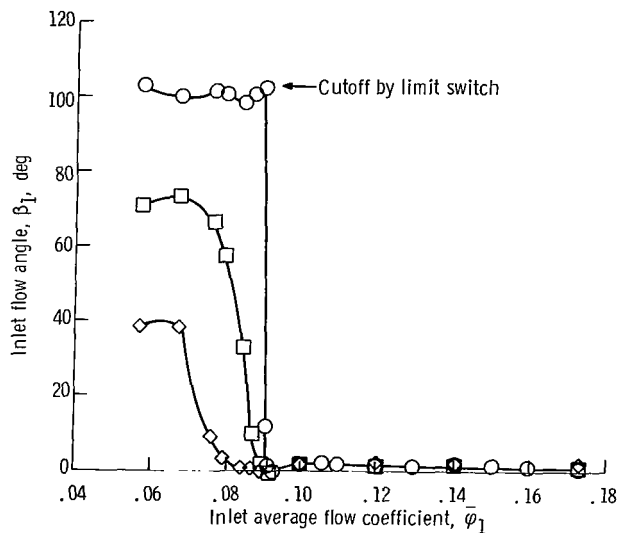
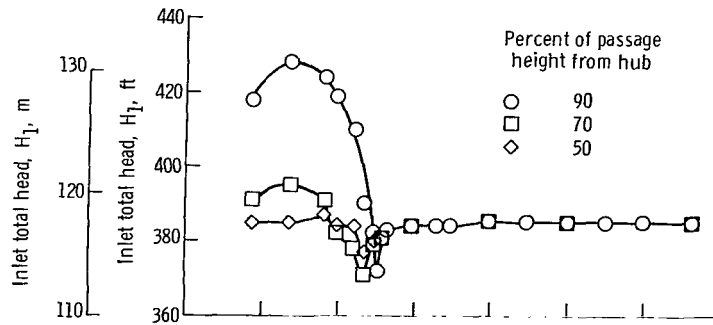


Figure 7. - Variation of inlet flow angle and total head with flow at three radial or passage height locations.

streamline flow until severe flow shifts occur across the blade row.

One occasion for severe flow shifts across the inducer occurs when the eddy forms in the blade inlet tip region. Under these flow conditions, the assumed streamlines used to calculate flow parameters in the tip region will vary markedly from the actual streamline flow, and parameters based on measurements at blade inlet and outlet of the blade row will have little meaning. For this reason, some local values of parameters in the blade tip region are omitted in subsequent plots.

The noncavitating blade-element performance is presented in figure 8 as radial distributions of flow and performance parameters at four average flow coefficients. All the parameters are defined in the list of symbols (appendix A) or in the list of equations (appendix B). The flow into the inducer was axial ( $\beta_1 = 0$ ) except when an inlet eddy was detected. The incidence angles presented are based on the estimated mean camber line blade angles listed in table I.

Design flow operation: Detailed performance of the blade elements near design flow operation is studied from the parameter distributions at an average flow coefficient of 0.105. At the inducer inlet, the small radial variations of  $\phi_1$  (see fig. 8) indicate some slight streamline curvature effects. Both the hub and tip are tapered across the inducer, and this is reflected in the  $\phi_1$  distribution.

The performance parameters of primary interest are the head rise and efficiency. The radial distribution of  $\psi$  (fig. 8) shows a slightly increasing  $\psi$  from hub to tip. The head-rise coefficient at the tip blade element was slightly higher than the design value of 0.303, whereas over the rest of the blade span, it was slightly below the design head rise. The efficiency of the flow process (fig. 8) was highest (approx 97 percent) in the hub region and decreased with radius to a value of approximately 78 percent at the tip element. These distributions of  $\psi$  and  $\eta$  result from the relative effects of energy addition and loss.

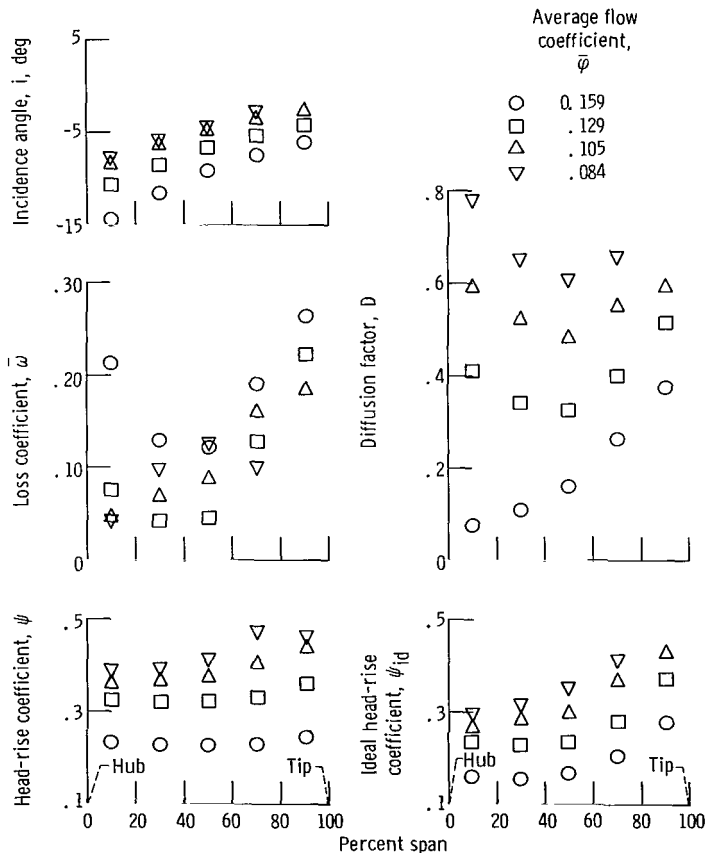


Figure 8. - Radial distributions of blade-element parameters under non-cavitating flow conditions. Rotor tangential velocity at outlet tip, 146 feet per second (44.5 m/sec); net positive suction head, 384 feet (117 m).

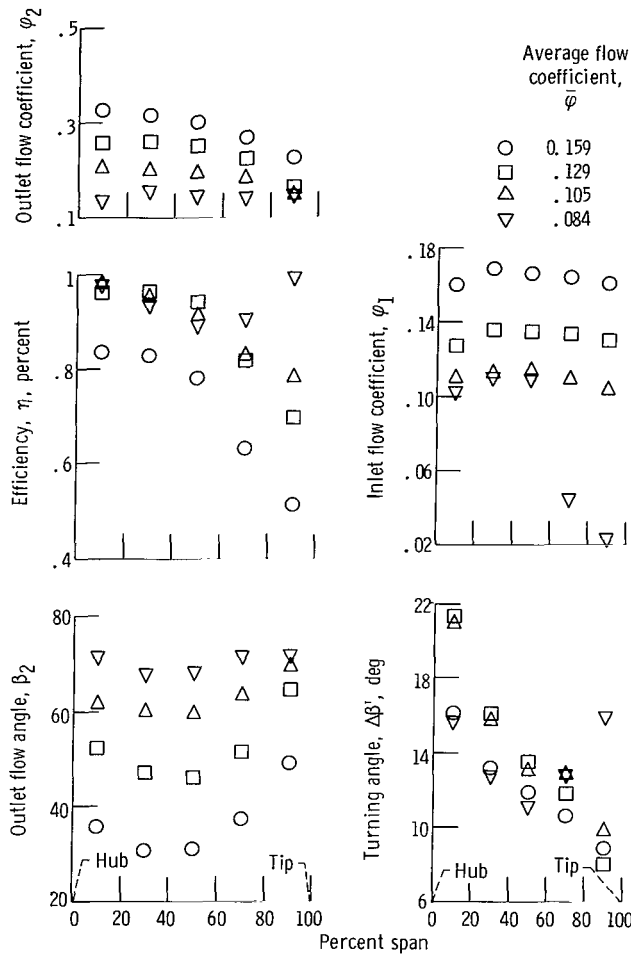


Figure 8. - Concluded.

At this near-design operation, the radial distribution of energy addition  $\psi_{id}$  (fig. 8) shows a relatively sharp increase in  $\psi_{id}$  from hub to tip. This type of distribution is typical of blades composed of radial elements where the design energy additions can be specified at just one blade element. It is also notable that over the portion of the blade span from the hub to the mean, the ideal head-rise coefficient  $\psi_{id}$  was less than the design overall head-rise coefficient. One reason, then, for not quite attaining the design level of head-rise coefficient in this inducer was that the energy addition was slightly low. It would be desirable to increase the energy addition through higher fluid turning in the hub and mean regions only; however, for a blade composed of radial elements such as in this design, the level of energy addition would have to be increased over the entire blade span.

The blade-element loss coefficient  $\bar{\omega}$  also indicates a sharp increase from hub to tip. This radial distribution is attributed to the secondary flow effects, in particular,

the centrifuging of blade surface boundary layer. Without three-dimensional flow effects, the loss level would be expected to vary with the blade loading, which reflects the blade surface boundary layer growth. A measure of the blade loading of each element is given by the diffusion factor  $D$  (fig. 8). Associating the blade loading ( $D$ ) levels of each blade element with its corresponding loss level indicates the strong influence of the secondary flow effects on the radial distribution of loss. For example, the  $D$ -factor for the hub and tip blade elements (for  $\bar{\omega} = 0.105$ ) are the same, but the  $\bar{\omega}$  of the tip element is approximately four times higher than the  $\bar{\omega}$  for the hub element flow.

The combining effects of  $\psi_{id}$  and  $\bar{\omega}$  are to achieve a nearly constant radial distribution of inducer head-rise coefficient  $\psi$ . As noted, all the blade-element parameters are interrelated and interact in such a way as to establish radial equilibrium. For example, although the losses and energy additions were presented as being essentially independent, the loss distributions do affect the outlet flow coefficient variation which, in turn, affects the energy addition distribution.

Some assessment of the parameter levels measured in the tandem-bladed inducer can be made by comparing them with similar values obtained at near-design operating

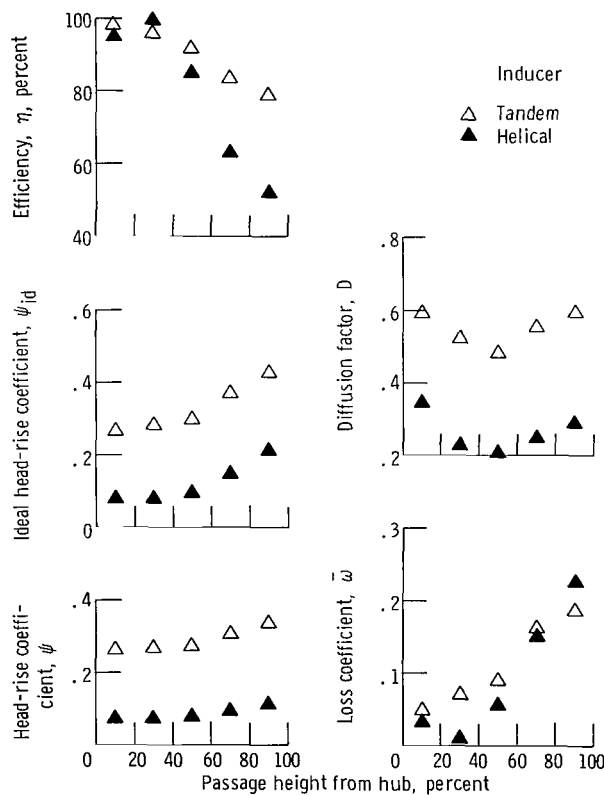


Figure 9. - Comparison of blade-element parameters from tandem-bladed inducer and 80.6° flat-plate helical inducer of reference 5.

conditions for the typical flat-plate inducer reported in reference 5. These comparisons are made in figure 9.

The plots show that the blade loading  $D$ , the energy addition  $\psi_{id}$ , and head rise  $\psi$  of the tandem-bladed inducer are all from two to three times that obtained with the constant lead, helical inducer. Comparison of the losses  $\bar{\omega}$  indicates no significant increase in loss level despite the higher loading levels of the tandem-bladed inducer. Apportioning the overall loading between the two separate blade rows has evidently prevented any serious separation of blade surface boundary layer and therefore diffusion losses. Both inducers showed similar radial distributions for all parameters. As a result of the relative levels of  $\psi_{id}$  and  $\bar{\omega}$ , the efficiency of the tandem-bladed inducer is generally higher than that of the helical inducer, particularly in the blade tip region.

A matter for concern with a highly loaded rotor is the losses incurred in the accompanying downstream stator that converts the kinetic energy of flow leaving the rotor to static pressure and sets up required velocity diagrams in a succeeding rotor. With the use of the outlet flow angles from the inducer, approximate values of D-factor for flow across a tip, mean, and hub blade element of a stator blade row were calculated. The results, together with assumptions of blade-section solidity  $\sigma$  and the axial velocity change across the stator, are shown in table II.

In table II, the stator row was assumed to turn the flow to the axial direction ( $\beta_{out} = 0$ ). With no axial velocity change across the stator, the D-factors are high ( $>0.6$ ), particularly in the blade tip region, and high losses could be expected with a single blade row. Some decrease in  $D$  could be realized by increasing the solidity  $\sigma$ , but practical limitations would keep any decrease from this source small. A more desirable approach is to increase the axial velocity across the stator row. The higher axial velocity leaving the stator lowers the stator diffusion and benefits the hydrodynamic

TABLE II. - CALCULATED DIFFUSION FACTORS  
FOR SUCCEEDING STATOR BLADE ROW

Span location	Flow angle, deg		Blade solidity, $\sigma$	Axial velocity ratio, $V_{z, out}/V_{z, in}$	Diffusion factor, D
	$\beta_{in}$	$\beta_{out}$			
Tip	70	0	1.5	1.0	0.9711
Mean	60	0	2.0	1.0	.7164
Hub	62	0	2.5	1.0	.7070
Tip	70	0	1.5	2.0	0.6291
Mean	60	0	2.0	2.0	.2164
Hub	62	0	2.5	2.0	.2375

design of the succeeding high pressure stages (see ref. 6). The flow coefficient leaving the inducer rotor is approximately 0.2. This coefficient could be increased from two to three times across a stator row. As indicated in table II, using an axial velocity ratio of 2 across the stator row generally brings the stator D-factors within reasonable levels for a single-vane blade row.

Off-design flow operation: As flow through the tandem-bladed inducer is increased from the design level, the incidence angles are decreased uniformly over the blade span (fig. 8). The radial distributions of  $D$ ,  $\psi_{id}$ , and  $\psi$  show reductions at all radii, as would be anticipated. Loss coefficient  $\bar{\omega}$  and turning angle  $\Delta\beta'$  show quite significant changes across the passage.

The most notable change in losses as flow is increased from the design value occurs in the hub region. At the highest flow rate ( $\bar{\varphi} = 0.159$ ), the loss across the hub element is increased sharply over the design flow level. A similar trend of hub loss with an increase in flow is noted in the loss values for the flat plate helical inducer of reference 5.

The reason for the high losses in the hub region is not obvious. The low-momentum fluid is apparently not being centrifuged from the hub region, as appeared to be the case near design flow. Also, the loss level appears high for the relatively low D-factor determined for flow in this region. The probable source of these losses appears to be the high negative incidence angle of the entering flow. In this case, the greater flow accelerations and decelerations with the associated losses would occur on the blade pressure surface near the blade leading edge. Because passage secondary flow patterns tend to move toward the hub along the blade pressure surface, the tendency would be to keep any losses formed on the blade pressure surface (near the hub) in this region. In these speculations, the flow about a tandem-blade element is considered from the same approach to flow about a single solid blade. With tandem-blade sections, the loss may be more intimately associated with the blade surface velocity gradients (local D-factor) of either the front or rear blade row, depending on the blade loading split between the two blade sections and the way the velocity gradients on each individual blade section react to a change in incidence angle.

From the blade mean section to the blade tip section, the loss coefficient showed a rapid increase with radius similar to that noted at design flow. The loss levels were higher at all radii than those measured near the design flow rate.

At the high flow ( $\bar{\varphi} = 0.159$ ), the blade-element turning angle  $\Delta\beta'$  was lower at all blade sections than that measured near the design flow. The decrease in fluid turning was roughly in the same proportion as the decrease in incidence angle, which indicated that deviation of flow from the blade camber line did not change significantly.

Flow conditions below design are studied from the parameter plots at  $\bar{\varphi} = 0.084$ . At this flow coefficient, an eddy was present in the blade inlet tip flow region (see fig. 7). Inlet flow measurements in or near the eddy are questionable, and the possible effects

on the parameter values should be recognized in assessing both the levels and distributions. Thus, the discussion of blade-element parameters at this low flow will be focused on the lower half (hub to mean) of the blade span.

The blockage effects of the eddy on the inlet flow distributions at  $\bar{\varphi} = 0.084$  are evident. The inlet flow coefficient  $\varphi_1$  drops off sharply to a zero value in the blade tip region. The major portion of the flow passes through the area from the blade mean to the blade hub. As a consequence, the local flow coefficients and incidence angles from hub to mean show little change with the reduction in flow.

Ordinarily, a reduction in flow without the presence of an eddy would increase the incidence angle of all blade elements until, at one or more blade sections along the span, the flow would separate from the blade suction surface near the blade leading edge. The blade sections at which this occurs are said to be stalled, and a significant decrease in head rise and efficiency occurs. The formation and radial growth of the eddy as flow is reduced cause a redistribution of inlet flow so that the local velocities into the lower portions of the blade span are large enough to prevent a stalling incidence angle from being attained. The net result is a continuing increase in overall head rise as flow is reduced. With the presence of an eddy flow region, the overall efficiency of the flow across the inducer would be expected to decrease. The blade-element efficiencies do not reflect this trend. It is likely that the flow measurements made herein do not account for certain parasitic losses associated with the eddy flow that would be observed from torque measurements.

At the low flow coefficient ( $\bar{\varphi} = 0.084$ ), significant redistribution of flow occurs within the blade passages (see  $\varphi_1$  and  $\varphi_2$  in fig. 8). Thus, the assumed blade-element flow will deviate more from the actual streamline flow at this operating condition than at the higher flow operation. In the hub region, the D-factor indicates a high diffusion rate ( $D_h = 0.78$ ); however, the losses remain at a relatively low level. This result is again attributed to secondary flow effects (probably the centrifuging of most of the blade surface boundary layer).

The blade-element plots at this low flow coefficient show a reduced (compared with those at design flow) turning angle  $\Delta\beta'$  (fig. 8). The inlet relative flow angle has varied only a degree or less from the design value (see plot for  $i$  at  $\varphi = 0.105$  in fig. 8) in the hub and mean span flow regions. This small variation indicates a greater deviation of flow from the outlet blade direction. The significant increases in flow deviation (particularly for the hub element) probably reflect some local separation on the more highly loaded rear blade section because of the high diffusion rate. As compared with the design levels, the lower turning angle tends to reduce the energy addition  $\psi_{id}$ , while the lower outlet flow coefficient  $\varphi_2$  tends to increase  $\psi_{id}$ . The net effect is a slight increase in  $\psi_{id}$  at all radii over the design level.

## Cavitating Performance

As the inlet pressure is decreased, local pressures through the blade passages are lowered to vapor pressure, and vapor cavities are formed. Cavitation is generally observed in the blade tip clearance flow and in flow along the blade suction surfaces. Cavitation on the blade suction surface has a more harmful effect on blade row performance. The cavities formed disrupt the normal streamline flow, thus affecting the energy addition to the fluid.

Overall performance. - The effect of cavitation on the inducer overall performance is shown in figures 10 and 11. The head-rise coefficient and efficiency are mass-averaged values. The average flow coefficient is based on the overall flow and the inlet flow area. The noncavitating base performance is shown for comparison. For the data of figure 10, the inlet net positive suction head is held constant and flow is varied,

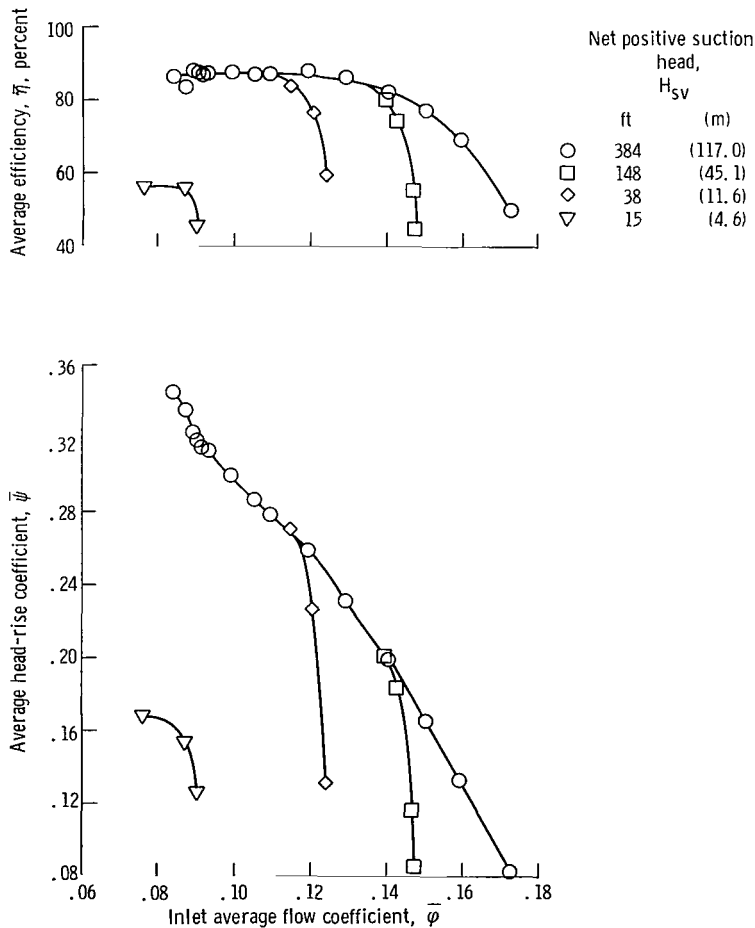


Figure 10. - Overall performance under cavitating and noncavitating conditions.

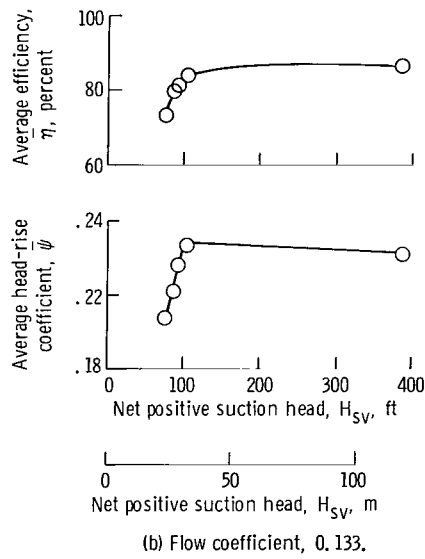
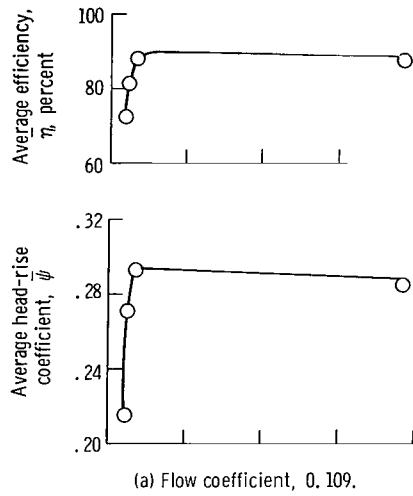
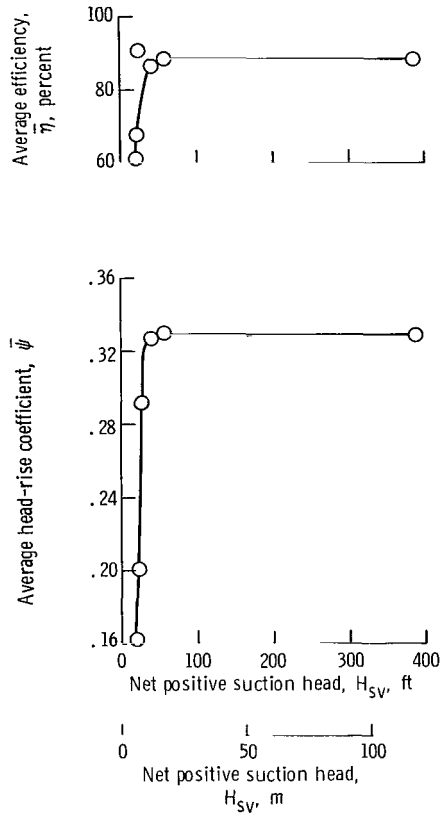


Figure 11. - Effects of cavitation on inducer overall head rise and efficiency.



(c) Flow coefficient, 0.092.

Figure 11, - Concluded.

whereas for figure 11, the flow is maintained constant and the inlet net positive suction head is varied. The overall performance plots indicate the average performance levels obtained by summing up the individual blade-element performances at a given operating point. The curves also permit orientation of a given operating flow with respect to the overall flow range covered.

Blade-element performance. - The plots in figure 12 compare the radial distributions of blade-element parameters as  $H_{sv}$  is decreased at a given  $\bar{\varphi}$ . Radial distributions are shown at three flows (below design, near design, and above design). The parameter values at the highest  $H_{sv}$  value shown are very close to the noncavitating values of figure 8 and are considered as noncavitating levels.

As  $H_{sv}$  was reduced, a blade surface cavity was observed to occur first on the upper half (from mean to tip) of the blade span and always covered a larger portion near the tip of the blade surface. All results of visual studies of cavitation in this inducer are reported in reference 1.

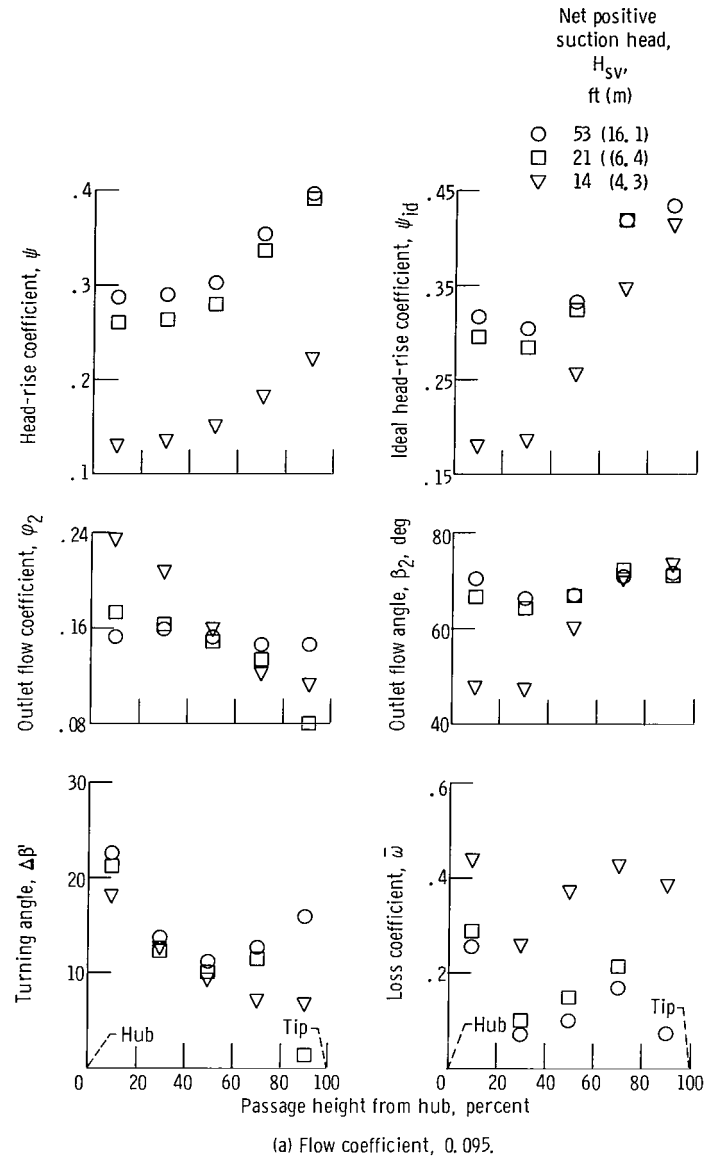
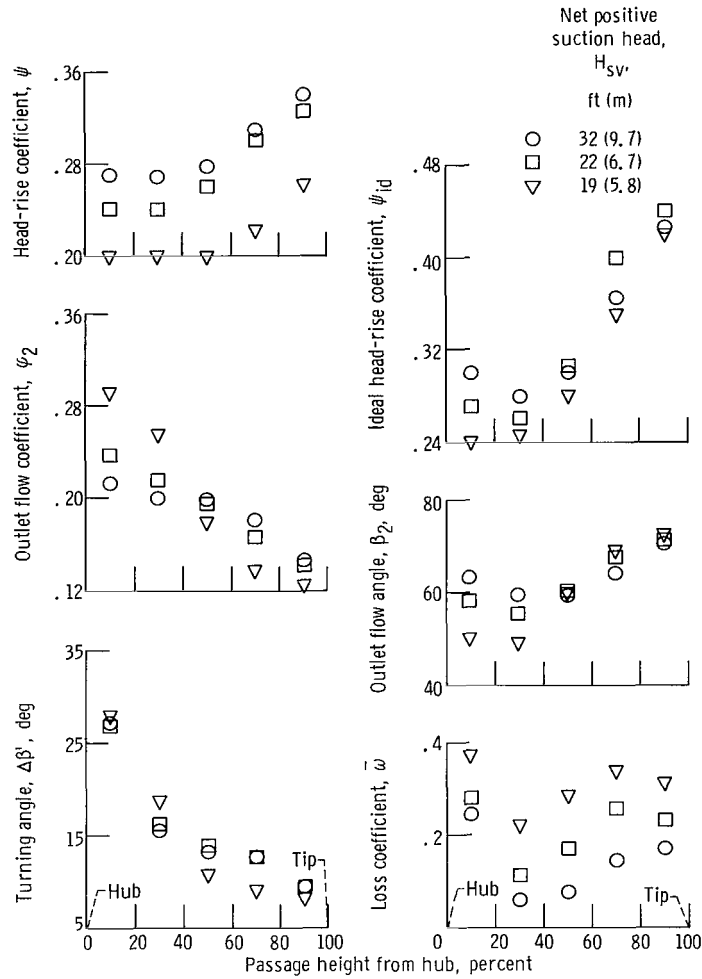


Figure 12. - Radial distribution of blade-element parameters under cavitating flow conditions.

The plots of figure 12 show that the effects of cavitation on blade-element performance are similar at all flows. However, the magnitude of the effects varies at the different flows because the changes in  $H_{sv}$  levels were not the same.

The parameter of primary interest is the head-rise coefficient. The radial distributions show that, as  $H_{sv}$  is decreased, the head rise is reduced for all blade elements along the span. This reduction in blade-element head rise could result from a decrease in energy addition  $\psi_{id}$  or an increase in loss  $\bar{\omega}$ . However, the effects of cavitation on  $\varphi_2$  are discussed prior to considering  $\psi_{id}$  or  $\bar{\omega}$ . The radial distributions of  $\varphi_2$  as

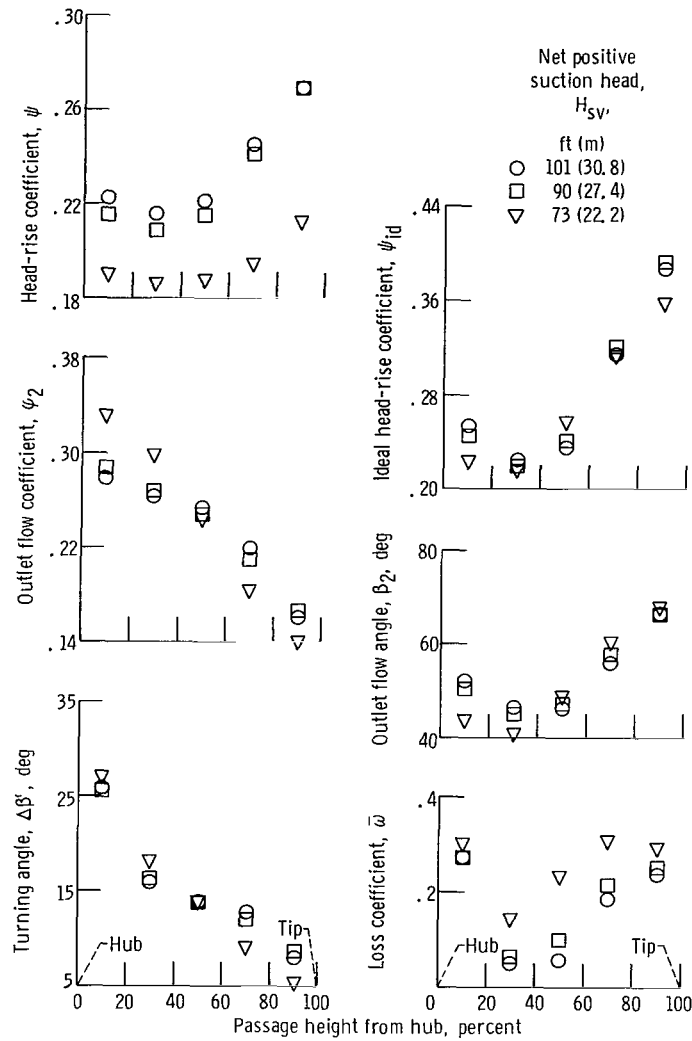


(b) Flow coefficient, 0.109.

Figure 12. - Continued.

$H_{sv}$  is lowered indicate that some redistributions of flow are occurring within the blade passage. The increase in  $\varphi_2$  in the hub region as  $H_{sv}$  is decreased indicates that an increasing portion of the flow is leaving the blade row in this region. The opposite trend is noted in the blade tip region. Evidently, the larger amount of cavitation in the tip flow regions provides an increased restriction to the flow, and an increasing proportion of the flow moves into the hub region flow area. Thus, in the tip flow regions, this reduction of  $\varphi_2$  tends to increase the  $\psi_{id}$ , while the converse occurs in the hub flow regions.

The other factor affecting  $\psi_{id}$  is the turning angle  $\Delta\beta'$ . Any change in  $\Delta\beta'$  tends to change  $\psi_{id}$  in the same direction. Two factors which would tend to reduce the fluid turning angle  $\Delta\beta'$  would be (1) a cavity on the blade surface that would reduce the effective camber of the blade sections and (2) high loss levels that are an indication of



(c) Flow coefficient, 0.130.

Figure 12. - Concluded.

some separation of boundary layer flow. The data of figure 12 show that the value of  $\Delta\beta'$  in the flow region from the blade mean to the blade tip decreases as  $H_{sv}$  is decreased. The lower  $H_{sv}$  level indicates an increase in the cavitation present, and the  $\bar{\omega}$  plots (fig. 12) show that  $\bar{\omega}$  increases as  $H_{sv}$  is decreased. Thus, both the aforementioned factors are affecting the fluid turning  $\Delta\beta'$ .

The reason for the slight increase in  $\Delta\beta'$  in the hub region as  $H_{sv}$  is decreased is not immediately apparent. The significant axial velocity increase across the blade elements in this region may have a favorable effect on deviation of the flow from the blade trailing edge direction, that is, may decrease the flow deviation and thus increase the  $\Delta\beta'$ . The net effect of  $\Delta\beta'$  and  $\varphi_2$  on  $\psi_{id}$  is shown in figure 12. In the hub region,

the increasing  $\varphi_2$  unloads these blade sections so that the  $\psi_{id}$  continues to decrease as  $H_{sv}$  is reduced. In the tip regions, the lower  $\varphi_2$  first results in an increase of  $\psi_{id}$ , but the reduced turning then causes  $\psi_{id}$  to fall beneath the noncavitating level.

As the  $H_{sv}$  is reduced, the  $\bar{\omega}$  increases across all blade elements along the blade span. The increase in  $\bar{\omega}$  with cavitation is generally associated with the mixing and flow deceleration downstream of the cavity collapse location.

## Some Effects of Slot Configuration

In the design inducer configuration, the trailing edge of the front blade and the leading edge of the rear blade lie in the same meridional plane (see fig. 2). This configuration is referred to as tandem I. Small changes to the slot geometry were made by moving the rear blade circumferentially approximately 0.1 inch (0.25 cm) from this design plane, both opposite to the direction of rotation (tandem II) and in the direction of rotation (tandem III). These changes in slot configuration can be visualized from the

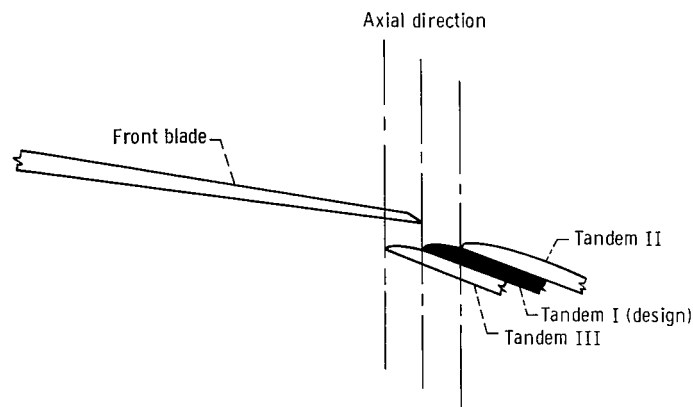
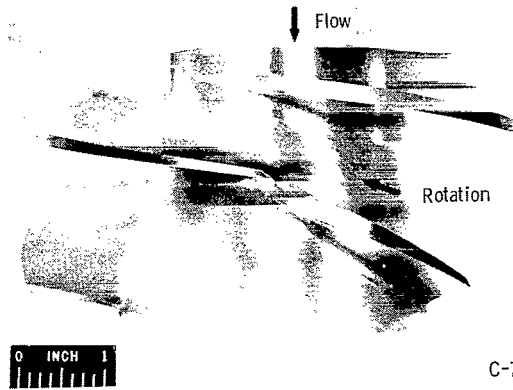


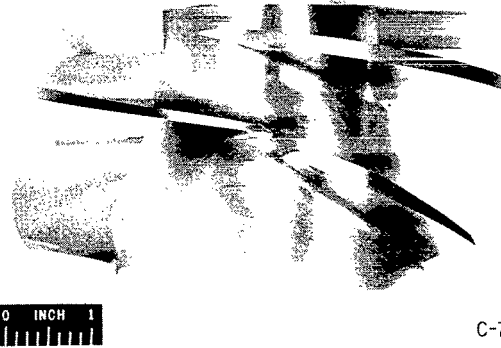
Figure 13. - Changes in slot geometry as rear blade of tandem inducer is moved circumferentially (not to scale).

sketch shown in figure 13 and the photographs of figure 14. The effects of these small geometry changes on selected blade-element parameters for noncavitating flow are shown in figure 15. For this phase of the investigation, measurements were taken across the midspan blade element only. The variations in head rise are generally small but consistent over the complete flow range. When the rear blade was moved in the direction opposite to the direction of rotation (tandem II), the head rise was slightly decreased from that produced by the design configuration (tandem I). When the rear blade was moved in the direction of rotation (tandem III), the head rise was slightly increased



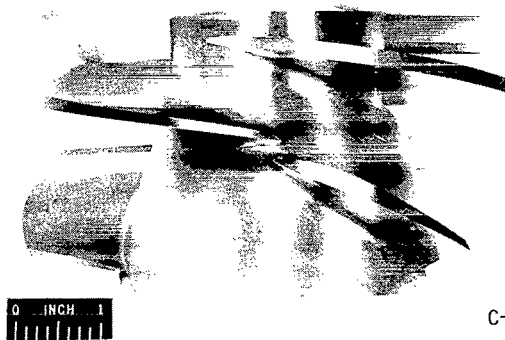
C-74607

(a) Tandem I. Design configuration.



C-74608

(b) Tandem II. Rear vane moved opposite to direction of rotation.



C-74605

(c) Tandem III. Rear vane moved in direction of rotation.

Figure 14. - Tandem-bladed inducer with rear vane in three circumferential locations.

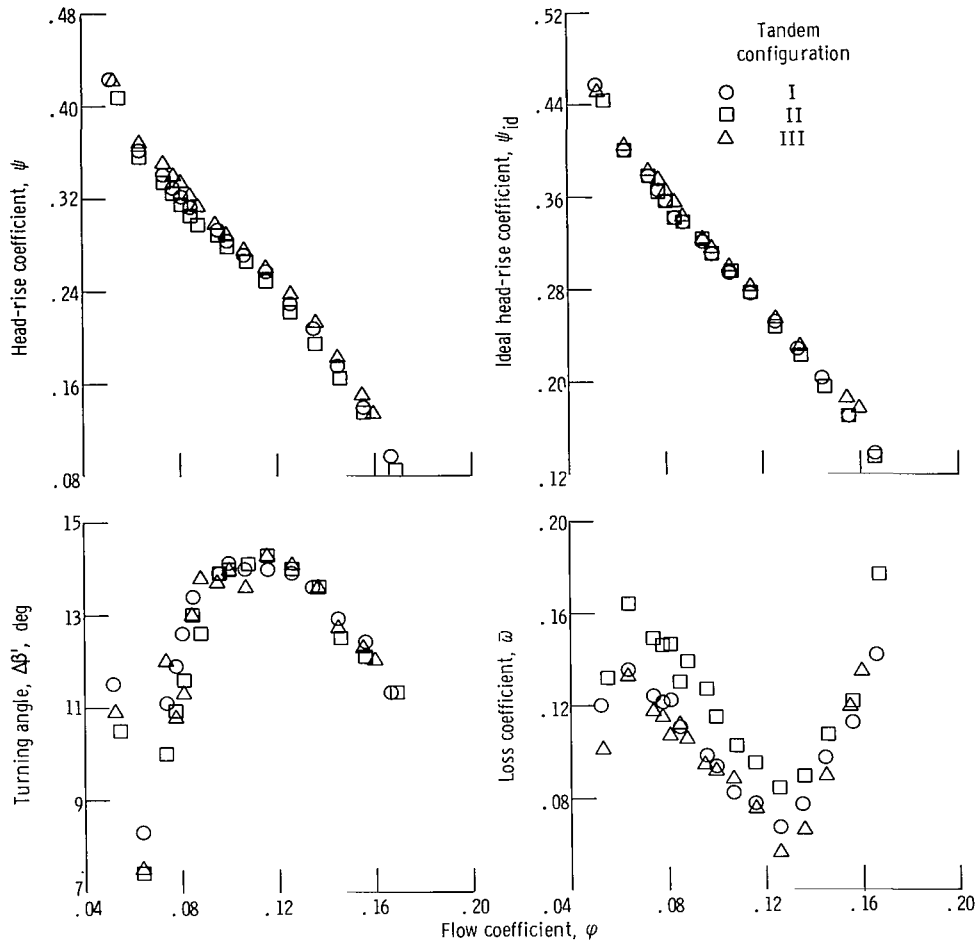


Figure 15. - Effect of slot geometry on mid-span blade-element parameters. Rotor tangential velocity at outlet tip, 146 feet per second (44.5 m/sec); net positive suction head, 384 feet (117 m).

from that produced by the design configuration.

No consistent trends of turning angle were noted over the entire flow range, which indicated that the changes in slot geometry had no measurable effect on the fluid turning done by this blade element. Over most of the operating range, the turning angles were within  $1/2^\circ$ . The energy addition  $\psi_{id}$  also shows little change between the three configurations.

The loss coefficient  $\bar{\omega}$  does show some variation with slot configuration. Tandem II indicates a higher loss coefficient over the entire flow range than that measured for the design configuration (tandem I). As the rear blade was moved in the direction of rotation (tandem III), a small decrease in loss coefficient compared with the level measured for the tandem I configuration is observed.

The plots of figure 15 indicate that the variation of head rise with slot geometry is caused primarily by the differences in flow losses. The configuration that had the greatest overlap of the two blades (tandem III) gave the lowest loss level.

## SUMMARY OF RESULTS

A tandem-bladed inducer was tested in water. The three-bladed inducer was 6.5 inches (16.5 cm) in diameter at the inlet, and the blade sections were formed by radial elements. The design inlet flow coefficient was 0.109 and the design head-rise coefficient was 0.303. The radial distributions of performance and flow parameters across individual tandem-blade elements were presented for both noncavitating and cavitating flow conditions.

At design flow the tandem-bladed inducer produced the design head rise in the blade tip region but produced a slightly lower head rise across the remaining portion of the blade span. No severe radial gradients of pressure or flow coefficient occurred at the inducer outlet. However, returning the flow to the axial direction (for a downstream stage) would require a very high diffusion rate without a significant increase in flow coefficient.

A comparison was made between parameter levels measured in the tandem-bladed inducer and a typical flat-plate helical inducer at near design operating conditions. The head rise of the tandem design was approximately twice the level attained with the flat-plate inducer. Also, for the tandem inducer, the efficiency remained at a higher level across most of the blade passage.

Loss coefficients increased significantly with radius at design and lower flows. These gradients were attributed to secondary flow effects, in particular, the centrifuging of blade surface boundary layer flows. As a result, blade-element efficiencies varied from about 97 percent at the hub to about 75 percent at the tip.

At flows below a flow coefficient of about 0.09, an eddy was detected in the tip region of the blade inlet. The radial extent of the eddy increased as flow was reduced. One result of the eddy formation was that most of the flow was redirected through the hub region, and stalling incidence angles in this region were not attained over the complete test flow range.

Cavitation resulted in a decrease in head rise at all blade elements along the blade span. The blade-element data indicated that, from the blade mean radius to the blade tip, cavitation had a more direct effect on the blade-element flow by increasing flow blockage and changing the effective blade camber. From the blade mean to the blade hub, the data indicated that the deterioration of performance results largely from the redistributions of flow because of the occurrence of cavitation. The decrease in head-rise

coefficient at all elements along the blade span resulted from both a decrease in energy addition and an increase in losses.

Midspan noncavitating performance data were taken with the rear blade at three different locations with respect to the front blade. As the overlap of the front and rear blades was increased, the measured losses decreased over the complete flow range. No consistent variation in turning angles was observed. Over most of the flow range, the turning angles of all three configurations compared within approximately  $1/2^\circ$ .

Lewis Research Center,  
National Aeronautics and Space Administration,  
Cleveland, Ohio, August 1, 1969,  
128-31.

## APPENDIX A

### SYMBOLS

<p>A area, in.<sup>2</sup>; cm<sup>2</sup></p> <p>D diffusion factor, eq. (B8)</p> <p>d diameter, in.; cm</p> <p>g acceleration due to gravity, 32.17 ft/sec<sup>2</sup>; 9.8 m/sec<sup>2</sup></p> <p>H total head, ft; m</p> <p><math>\Delta H</math> blade-element head rise, ft; m</p> <p><math>\overline{\Delta H}</math> mass-averaged head rise, ft; m</p> <p><math>H_{sv}</math> net positive suction head, ft; m</p> <p><math>h_v</math> vapor pressure head, ft; m</p> <p>i incidence angle, eq. (B9), deg</p> <p>j index number</p> <p>N rotative speed, rpm</p> <p>Q flow rate, gal/min; m<sup>3</sup>/min</p> <p><math>Q_v</math> Venturi-measured flow rate, gal/min; m<sup>3</sup>/min</p> <p>r radius, ft; m</p> <p><math>t_{max}</math> thickness, ft; m</p> <p>U rotor tangential velocity, ft/sec; m/sec</p> <p>V absolute velocity, ft/sec; m/sec</p> <p>x, y directional coordinates (defined in fig. 2), in.; cm</p> <p><math>\beta</math> flow angle, deg</p> <p><math>\Delta\beta'</math> turning angle, deg</p>	<p><math>\eta</math> hydraulic efficiency (eq. (B5)), percent</p> <p><math>\overline{\eta}</math> mass-averaged hydraulic effi- ciency (eq. (B14)), percent</p> <p><math>\kappa</math> blade angle, deg</p> <p><math>\sigma</math> blade solidity</p> <p><math>\varphi</math> flow coefficient</p> <p><math>\overline{\varphi}</math> average flow coefficient</p> <p><math>\psi</math> head-rise coefficient</p> <p><math>\overline{\psi}</math> mass-averaged head-rise coeffi- cient</p> <p><math>\overline{\omega}</math> rotor relative total head loss coefficient (eq. (B7))</p> <p><b>Subscripts:</b></p> <p>c cylinder</p> <p>h hub</p> <p>id ideal</p> <p>n radius position</p> <p>t tip</p> <p>z axial component</p> <p><math>\theta</math> tangential direction</p> <p>1 inlet</p> <p>2 outlet</p> <p><b>Superscript:</b></p> <p>' relative to rotor</p>
--	--

## APPENDIX B

### BLADE-ELEMENT AND PARAMETER EQUATIONS

#### Blade-Element Equations

Blade-element head rise:

$$\Delta H = H_2 - H_1 \quad (\text{B1})$$

Head rise coefficient:

$$\psi = \frac{g \Delta H}{U_t^2} \quad (\text{B2})$$

Ideal head rise:

$$\Delta H_{\text{id}} = \frac{U_2 V_{\theta, 2} - U_1 V_{\theta, 1}}{g} \quad (\text{B3})$$

Ideal head-rise coefficient:

$$\psi_{\text{id}} = \frac{g \Delta H_{\text{id}}}{U_t^2} \quad (\text{B4})$$

Hydraulic efficiency:

$$\eta = \frac{\Delta H}{\Delta H_{\text{id}}} \times 100 \quad (\text{B5})$$

Flow coefficient:

$$\varphi = \frac{V_z}{U_t} \quad (\text{B6})$$

Rotor relative total head loss coefficient:

$$\bar{\omega} = \frac{H'_{2, id} - H'_2}{\frac{V'_1{}^2}{2g}} = \frac{\Delta H_{r1} - \Delta H}{\frac{V'_1{}^2}{2g}} \quad (B7)$$

Blade diffusion factor:

$$D = 1 - \frac{V'_2}{V'_1} + \frac{r_2 V_{\theta, 2} - r_1 V_{\theta, 1}}{\sigma V'_1 (r_1 + r_2)} \quad (B8)$$

or, for  $r_1 = r_2$ ,

$$D = 1 - \frac{V'_2}{V'_1} + \frac{\Delta V_{\theta}}{2\sigma V'_1}$$

Incidence angle:

$$i = \beta'_1 - \kappa_1 \quad (B9)$$

Turning angle:

$$\Delta\beta' = \beta'_1 - \beta'_2 \quad (B10)$$

## Overall and Averaged Parameter Equations

Mass-averaged head rise:

$$\Delta H = \frac{\sum_{j=1}^{j=4} (r_j V_{z, 2, j} \Delta H_j + r_{j+1} V_{z, 2, j+1} \Delta H_{j+1})(r_j - r_{j+1})}{\sum_{j=1}^{j=4} (r_j V_{z, 2, j} + r_{j+1} V_{z, 2, j+1})(r_j - r_{j+1})} \quad (B11)$$

Mass-averaged head-rise coefficient:

$$\bar{\psi} = \frac{g \overline{\Delta H}}{U_t^2} \quad (\text{B12})$$

Mass-averaged ideal head rise:

$$\overline{\Delta H}_{id} = \frac{1}{g} \left( \overline{U_2 V_{\theta, 2}} - \overline{U_1 V_{\theta, 1}} \right) = \frac{1}{g} \left( \frac{\sum_{j=1}^{j=4} U_{2,j} V_{\theta, 2,j} A_{2,j} V_{z, 2,j}}{\sum_{j=1}^{j=4} A_{2,j} V_{z, 2,j}} - \frac{\sum_{j=1}^{j=4} U_{1,j} V_{\theta, 1,j} A_{1,j} V_{z, 1,j}}{\sum_{j=1}^{j=4} A_{1,j} V_{z, 1,j}} \right) \quad (\text{B13a})$$

In this investigation  $V_{\theta, 1}$  was considered zero in all calculations, and the equation becomes

$$\overline{\Delta H}_{id} = \frac{1}{g} \left( \frac{\sum_{j=1}^{j=4} U_{2,j} V_{\theta, 2,j} A_{2,j} V_{z, 2,j}}{\sum_{j=1}^{j=4} A_{2,j} V_{z, 2,j}} \right) = \frac{\overline{U_2 V_{\theta, 2}}}{g} \quad (\text{B13b})$$

Mass-averaged efficiency:

$$\bar{\eta} = \frac{\overline{\Delta H}}{\overline{\Delta H}_{id}} \times 100 \quad (\text{B14})$$

Average inlet axial velocity:

$$\bar{V}_{z, 1} = \frac{Q_v}{k\pi (r_{t, 1}^2 - r_{h, 1}^2)} \quad (\text{B15})$$

where  $k = 448.8$  feet per second or  $k = 60$  meters per second.

Average inlet flow coefficient:

$$\bar{\varphi} = \frac{\bar{V}_{z,1}}{U_t} \quad (\text{B16})$$

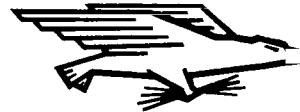
Net positive suction head:

$$\bar{H}_{sv} = \bar{H}_1 - h_v \quad (\text{B17})$$

## REFERENCES

1. Soltis, Richard F.; Urasek, Donald C.; and Miller, Max J.: Overall Performance of a Tandem-Bladed Inducer Tested in Water. NASA TN D-5134, 1969.
2. Raily, J. W.; and El-Sarha, M. E.: An Investigation of the Flow Through Tandem Cascades. Proc. Inst. Mech. Engrs., vol. 180, pt. 3J, 1965-1966, pp. 66-73.
3. Crouse, James E.; Montgomery, John C.; and Soltis, Richard F.: Investigation of the Performance of an Axial-Flow-Pump Stage Designed by the Blade-Element Theory - Design and Overall Performance. NASA TN D-591, 1961.
4. Leiblen, Seymour; Schwenk, Francis C.; and Broderick, Robert L.: Diffusion Factor for Estimating Losses and Limiting Blade Loadings in Axial-Flow-Compressor Blade Elements. NACA RM E53D01, 1953.
5. Sandercock, Donald M.; Soltis, Richard F.; and Anderson, Douglas A.: Cavitation and Noncavitation Performance of an 80.6° Flat-Plate Helical Inducer at Three Rotational Speeds. NASA TN D-1439, 1962.
6. Miller, Max J.; and Crouse, James E.: Design and Overall Performance of an Axial-Flow Pump Rotor with a Blade-Tip Diffusion Factor of 0.66. NASA TN D-3024, 1965.

FIRST CLASS MAIL



POSTAGE AND FEES PAID  
NATIONAL AERONAUTICS AND  
SPACE ADMINISTRATION

69321 00903  
OCT 28 1958  
ARMED SERVICES LABORATORY/WL117  
CANTON AIR FORCE BASE NEW MEXICO 87111

ALL INFORMATION CONTAINED HEREIN IS UNCLASSIFIED

POSTMASTER: If Undeliverable (Section 158  
Postal Manual) Do Not Return

*"The aeronautical and space activities of the United States shall be conducted so as to contribute . . . to the expansion of human knowledge of phenomena in the atmosphere and space. The Administration shall provide for the widest practicable and appropriate dissemination of information concerning its activities and the results thereof."*

— NATIONAL AERONAUTICS AND SPACE ACT OF 1958

## NASA SCIENTIFIC AND TECHNICAL PUBLICATIONS

**TECHNICAL REPORTS:** Scientific and technical information considered important, complete, and a lasting contribution to existing knowledge.

**TECHNICAL NOTES:** Information less broad in scope but nevertheless of importance as a contribution to existing knowledge.

**TECHNICAL MEMORANDUMS:** Information receiving limited distribution because of preliminary data, security classification, or other reasons.

**CONTRACTOR REPORTS:** Scientific and technical information generated under a NASA contract or grant and considered an important contribution to existing knowledge.

**TECHNICAL TRANSLATIONS:** Information published in a foreign language considered to merit NASA distribution in English.

**SPECIAL PUBLICATIONS:** Information derived from or of value to NASA activities. Publications include conference proceedings, monographs, data compilations, handbooks, sourcebooks, and special bibliographies.

**TECHNOLOGY UTILIZATION PUBLICATIONS:** Information on technology used by NASA that may be of particular interest in commercial and other non-aerospace applications. Publications include Tech Briefs, Technology Utilization Reports and Notes, and Technology Surveys.

*Details on the availability of these publications may be obtained from:*

SCIENTIFIC AND TECHNICAL INFORMATION DIVISION  
NATIONAL AERONAUTICS AND SPACE ADMINISTRATION  
Washington, D.C. 20546